View metadata, citation and similar papers at core.ac.uk
brought to you by CORE

Acta Polytechnica **55**(6):393–400, 2015
doi:10.14311/APP.2015.55.0393
© Czech Technical University in Prague, 2015
available online at http://ojs.cvut.cz/ojs/index.php/ap

FINITE ELEMENT ANALYSIS OF AORTAL BIFURCATION

Jakub Kronek[a,*], Rudolf Žitný[b]

[a] *Czech Technical University in Prague, Faculty of Mechanical Engineering, Department of Mechanics, Mechatronics and Biomechanics, Technická 4, 166 07 Prague, Czech Republic*

[b] *Czech Technical University in Prague, Faculty of Mechanical Engineering, Department of Process Engineering, Technická 4, 166 07 Prague, Czech Republic*

[*] corresponding author: Jakub.Kronek@fs.cvut.cz

Abstract. Arterial bifurcations loaded by internal pressure are significant stress concentrators. Increased mechanical stress inside the arterial wall probably accelerates pathogenic processes at these places. The stress concentration factor (SCF) depends mainly on geometry, loading and material. This paper presents a map of SCFs calculated by FEM aortic bifurcation in the aortic bifurcation region (AB), loaded by static internal pressure. The influence of geometry (aortic diameter, wall thickness, bifurcation angle, "non-planarity" angle and radius of apex), material properties and internal pressure were evaluated statistically by regression of FEM results. Two material variants were used (linear Hooke and hyper elastic Ogden). Viscoelastic behaviour, anisotropy and prestrain were neglected. The results indicate that the highest Mises stress appears in the inner side of the AB apex, and that the SCF is negatively correlated with the bifurcation angle and with the internal pressure. The SCF varies from 4.5 to 7.5 (Hooke) and from 7 to 21 (Ogden).

Keywords: stress concentration factor; aorta; artery; bifurcation; branching.

1. Introduction

Atherosclerosis is a major cause of death in the western world [1, 2]. For a successful fight against this disease of civilisation, it is crucial to understand the processes that lead to or accelerate atherosclerosis. Many biomechanical works [3–13] have dealt with the interaction between blood flow and the intimal surface of the arteries in the region of arterial bifurcation or branching. It has been shown that very low wall shear stress (less than 1 Pa) accelerates the formation of atherosclerotic lesions in these regions [8, 14]. Other works [15, 16] have indicated that a high level of transmural pressure, which causes tensile stress inside the arterial wall, may also cause degenerative atherosclerotic changes. Arterial bifurcations are significant geometrical stress concentrators, which increase the mechanical stress many times in comparison with the level in non-branched regions. The stress concentration factor (SCF) is the ratio of the maximum stress and the nominal stress in a non-branched artery. According to [17], the SCF within carotid bifurcation may reach values more than 30. Other analyses of SCF have been published in [18–20]. SCF depends on many factors. Firstly, the geometry of the bifurcation. The loading and the material properties also have an impact. The aim of our work is to find simple correlations for peak stresses and SCF using only a small number of parameters (geometry, material, internal pressure). The aortal bifurcation was chosen as suitable representative of arterial bifurcations.

2. Methods

It is hard to measure stress directly within the arterial wall, so we used finite element (FE) modelling of aortic bifurcations. A description of the AB geometry using a minimum number of parameters was the most important aspect of the design of the FE models. For this purpose, we carried out a literature review, and supplemented it by our own measurements on cadavers. We attempted to select independent geometrical parameters and/or to find a statistically relevant relation between two or more geometrical parameters, e.g. the relation between the diameter of the abdominal aorta (AA) and the diameters of common iliac arteries (CIA)

2.1. Geometry of AB

AB is the terminal part of AA, which divides the blood flow between the left CIA and the right CIA. The geometry of AB generally corresponds to a slightly non-planar Y-shaped bifurcation (non-planarity is characterised by angle β). The bifurcation angles of the left CIA (αL) and the right CIA (αR) may be identical, but this is not necessarily. The transition between AA and CIA is gradual, and may be characterised by the radius of an osculating circle (rL, rR), see Fig. 1. Both AA and CIA generally have an elliptical (oval) cross-section. Another non-uniformity may be caused by the fact that the wall thickness is not constant. An offset of the left and right CIAs may also be observed in some patients.

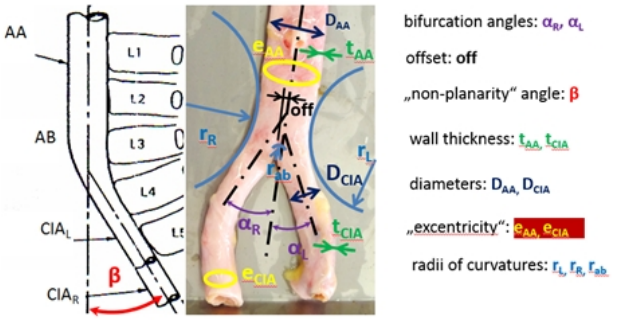

Figure 1. Schematic illustration of AB geometry with geometrical parameters marked.

Some papers have presented measured values of angles α and β [21–25], diameters of AA and CIA [21, 22, 25, 26], wall thicknesses [27–29], eccentricity [25, 27] and radii of curvature [21, 22] (Figure 1, Table 1).

2.2. Experimental measurements of geometries

Measurements of 12 human ABs resected from cadavers (age from 17 to 71 years) were made during autopsies in the Department of Forensic Medicine of the Kralovske Vinohrady University Hospital. The relevant ethical committee approved the use of human tissue in this study. Each sample was photographed, together with a length scale for evaluating the scale factor and the real dimensions (software ImageJ was used for processing the pictures). The axis of AA and the branches were identified more or less manually. The evaluated geometrical parameters, together with results published by other authors, are presented in Tab. 1 (angles β could not be evaluated from the photographs). Non-dimensional eccentricity e_{AA} is defined as the maximum diameter (usually in lateral direction) divided by the minimum diameter (usually in antero-posterior direction).

On the basis of our own measurements on 12 cadavers, estimates were made of the mean values of diameters $D_{AA} = 13.8\,\text{mm}$ and $D_{CIA} = 8.7\,\text{mm}$, with standard deviations $s_{DAA} = 4.5\,\text{mm}$ and $s_{DCIA} = 3.8\,\text{mm}$. The inner diameters could not, of course, be evaluated from in situ photographs. It was necessary to use a different technique, based on extracted bABs, in the form of excised circular rings. The mean diameters were evaluated from the lengths of the rings. The rings were also used for evaluating the wall thickness profiles (circular rings were cut and then stretched into strips, the thickness of which was measured using a laser scanner (Microepsilon). A significant correlation $t_{CIA} = 0.89\,t_{AA}$ was observed (α-value < 0.01). A statistically evaluated reduction of diameters $D_{CIA} = 0.64 D_{AA}$ seems to be a reasonable approximation of the Murray law [30] (the principle of minimised dissipated energy and metabolic consumption) and the EGM principle (Entropy Generation Minimisation).

Source	n	Age (years)	α (°)	β (°)	D_{AA} (mm)	D_{CIA} (mm)	t_{AA} (mm)	t_{CIA} (mm)	r_L, r_R (mm)	e_{AA} (1)
[21, 22]	37	71 ± 16	50 ± 16	18 ± 8	18.3 ± 3.8	10.9 ± 2.1	—	—	45	—
[23]	70	57 ± 16	35 ± 11	—	—	—	—	—	—	—
[24]	20	—	—	9.1 ± 5.6	—	—	—	—	—	—
[25]	12	27 to 84	34 ± 13	9.4	15.8	10.5	—	—	—	0.89
[26]	11	63 ± 9	—	—	18.5 ± 1.2	8.0 ± 2.4	—	—	—	—
[27]	11	0 to 76	—	—	—	—	1	—	—	0.9
[28]	196	45 to 84	—	—	—	—	2.2 ± 0.5	—	—	—
[29]	2466	19 to 67	—	—	—	—	1.8 ± 0.2	—	—	—
Our measurements on cadavers	12	51 ± 17	55 ± 15	—	13.8 ± 4.5	8.7 ± 3.8	1.8 ± 0.4	1.6 ± 0.4	—	—

Table 1. Geometrical parameters of AB evaluated from published works, together with and our own measurements on cadavers.

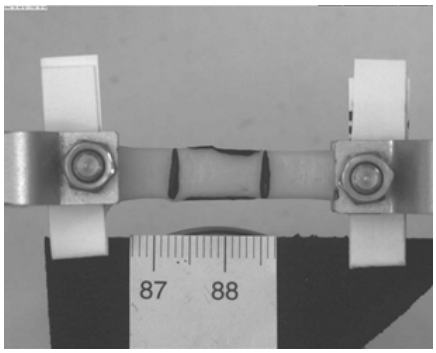

FIGURE 2. A fixed sample during the uniaxial tensile test.

2.3. EXPERIMENTAL MEASUREMENTS OF MATERIAL PROPERTIES

The mechanical properties of the arterial wall strips excised from the AB samples (the same samples as those used for evaluating the geometrical parameters) were identified in experiments carried out on a tensile testing machine for soft tissues (Messphysik Materials Testing GmbH, Fürstenfeld, Austria) equipped with a 100 N load cell. The ends of the strips were fixed by two clamps with pins (Figure 2). The samples were preconditioned by 4 loading cycles up to deformation of approximately 15 % before ultimate failure loading.

The deformations of the stretched strips were obtained via an image analysis of video records performed by a Matlab script that was developed in-house. The mechanical properties (described by an isotropic linear Hookean model and alternatively by a hyper elastic Ogden constitutive equation) were identified using a regression analysis of the stress strain data. The two-parametric Ogden model [31] was defined by the following strain energy function

$$W = \frac{2\mu}{\alpha^2}(\acute{\lambda}_1^{\alpha} + \acute{\lambda}_2^{\alpha} + \acute{\lambda}_3^{\alpha} + \frac{1}{D}(J^{el} - 1)^2,$$

where $\acute{\lambda}_i^{\alpha}$ are deviatoric principal stretches, J^{el} is elastic volume deformation. The model parameters for individual samples were identified by a Mathcad script and were averaged, giving mean values $\mu = 0.119\,\mathrm{MPa}$, $\alpha = 21.99$, $D = 0.338$ for the Ogden model and the Young modulus of elasticity $E = 1.6\,\mathrm{MPa}$ and the Poisson constant $\nu = 0.49$ for the linear Hooke model. More details are presented in [32].

2.4. FE MODELS

Thirty-two different geometries of FE models were created in Autodesk Inventor 2012 3D modelling software, using standard modelling tools (2D sketching, extrude, sweep along a line, chamfer of edges) and were exported to the Abaqus FE program. The 32 geometries have different combinations of the five most important geometrical variables $D_{AA} \approx (10\text{–}18)\,\mathrm{mm}$, $t_{AA} \approx (0.8\text{–}2.4)\,\mathrm{mm}$, $r_{AB} \approx (0\text{–}2.8)\,\mathrm{mm}$, $\alpha \approx (18\text{–}82)°$, $\beta \approx (0\text{–}32)°$; these parameters were distributed according to the principles of RSM (Response Surface Methodology). Other geometrical parameters were either correlated with the varying parameters $t_{CIA} = 0.89t_{AA}$, $D_{CIA} = 0.64D_{AA}$, or were fixed $e_{AA} = e_{CIA} = 0.9$, $r_R = r_L = 45\,\mathrm{mm}$.

The values and correlations were selected on the basis of a previous geometrical study. These 32 geometries did not correspond directly to any measured AB. The geometrical parameters of the models are chosen only to be within the ranges evaluated in a previous morphometric study.

For each geometry, Abaqus calculated the stress distributions (and therefore the SCFs) at a constant systolic pressure load of 120 mmHg, using alternately the Hooke model and the Ogden model , and using the material parameters presented in the previous paragraph (thus the same material parameters and the same load were applied for all 32 geometries).

The reference load of 120 mmHg is so high that the geometrical nonlinearities and also the material nonlinearities are significant (typical tangential stretches corresponding to this pressure are up to 1.2). In order to assess the effects of large deformations and the limit of the linear range, five typical geometries were selected and calculated, with internal pressures rising from 100 mmHg up to 190 mmHg.

The effect of the variability of the material parameters was tested only for the linear Hooke model: in addition to the reference values ($E = 1.6\,\mathrm{MPa}$, $\nu = 0.49$) the Young elastic modulus was varied from $E = 0.6\,\mathrm{MPa}$ to $26\,\mathrm{MPa}$ for four typical geometries and for a reference load of 120 mmHg for constant $\nu = 0.49$, because the aortic wall is practically incompressible, and lower Poisson constant values are of no practical significance. Numerical experiments indicate that SCFs calculated at the highest stiffness ($E = 26\,\mathrm{MPa}$) are close to but not exactly within the linear region.

3D quadratic brick elements C3D20R were used to create a mesh. The mesh was mapped in each case to ensure the same mesh density (5 elements to the wall thickness and 0.1mm width of the first element from the plane of symmetry in the region of the apex). In addition, a mesh convergence test was carried out with one selected geometry. Five meshes were created (from very thin to very dense) and two mesh density parameters were defined. The first parameter is the total number of elements, and the second parameter is the reciprocal of the width of the first element (which is normally 0.1 mm). The solution (Mises stress) converged with the two mesh density parameters (Figure 3).

The calculated Mises stress was tracked on two 1D paths. Path 1 leads from the highest stress peak in the apex caudally on the inner surface of CIA (Figure 4). Path 2 leads from the second stress peak in the outer rear side of AB cranially on AA (Figure 4).

Three variables were evaluated from each path: the maximum Mises stress in the stress concentrations at the beginnings of the path (σ_{max1}, σ_{max2}), the nomi-

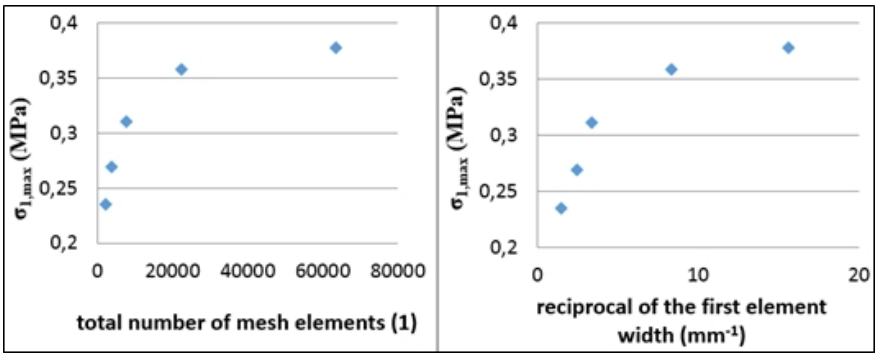

Figure 3. Test of mesh convergence. The solution (the highest Mises stress value in the apex of bifurcation) as a function of the first and second parameter of mesh density.

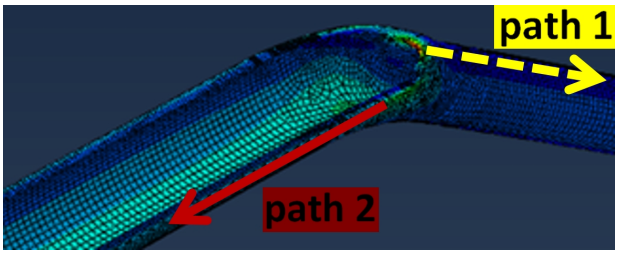

Figure 4. The stress was tracked on two paths. The figure shows the starting points and the direction of the paths.

nal (stable) Mises stress (σ_{nomin1}, σ_{nomin2}), and the distances from the beginning of the paths (l_{K1}, l_{K2}), where the stress drops almost to its nominal value ($\sigma < 1.1\sigma_{nomin}$). Stress concentration factors K_1 and K_2 were evaluated simply as $K_1 = \sigma_{max1}/\sigma_{nomin1}$ and $K_2 = \sigma_{max2}/\sigma_{nomin2}$.

2.5. Analytical approximation of SCF, maximum stresses and range

It is assumed that the following factorisation of pressure, material parameters and geometry can be used for a quick estimate of SCF:

$$K_1 = f_1(p,E)g_1(\alpha,\beta,d_{AA},t_{AA},r_{AB}),$$
$$K_2 = f_2(p,E)g_2(\alpha,\beta,d_{AA},t_{AA}),$$

where the pressure correction factor fi is a linear function $f_i = 1 + f_{i0}\frac{p}{E}$. The pressure correction factor is defined for the Ogden model as $f_i = 1 + f_{i0}\frac{p}{\mu}$ even if the FE calculations were performed with only one set of Ogden model parameters, therefore only for $\mu = 0.119\,\mathrm{MPa}$.

The geometric factor was suggested in linear form (linear with respect to the selected base functions). The use of dimensionless base functions reduces the number of parameters to five (K_1) or four (K_2):

$$g_1 = a_{10} + a_{11}\frac{D_{AA}}{t_{AA}} + a_{12}\cos^2\frac{\alpha}{2} + a_{13}\sqrt{1-\cos\beta} + a_{14}\frac{r_{AB}}{D_{AA}},$$

$$g_2 = a_{20} + a_{21}\frac{D_{AA}}{t_{AA}} + a_{22}\cos^2\frac{\alpha}{2} + a_{23}\sqrt{1-\cos\beta}.$$

The basis function $\sqrt{1-\cos\beta}$ was suggested by analogy with a pressurised bent pipe, and the basis function $\cos^2\frac{\alpha}{2}$ was motivated by the method which estimates the stresses in the apex using membrane behaviour [33]. The resulting analytical model has 6 dimensionless parameters (f_{i0}, a_{i0}, a_{i1}, a_{i2}, a_{i3}, a_{i4}), which were identified by regression analysis (modified Newton method) of approximately 120 SCF values calculated by Abaqus for the Hooke model (32 different geometries at a reference pressure of 120 mmHg and for reference material parameters + different pressures and different modulus of elasticity for three geometries) and about 90 SCF values calculated for the Ogden model (only 16 geometries, 6 of them with varying pressure and only one set of material parameters).

The two identified sets of parameters make it easy to estimate the four SCF values (separately for the Hooke model and for the Ogden model, and separately for the inner surface of CIA and for the outer surface of AA). These values also enable quick estimates of the maximum Mises stresses based on the nominal membrane stresses

$$\sigma_{1,max} = K_1\frac{pD_{CIA}}{2t_{CIA}}\phi_1, \quad \sigma_{2,max} = K_2\frac{pD_{AA}}{2t_{AA}}\phi_2$$

The value $\varphi_i = 1$ corresponds to thin circular tubes. A more accurate estimate can be based on an analytical solution of a pressurized elastic (and incompressible) elliptical pipe [34] with the correction factor φ corresponding to known eccentricity e, relative thickness and relative pressure:

$$\varphi_1 = 1 + \frac{3}{2}\frac{D_{CIA}}{t_{CIA}}\frac{1-e_{CIA}}{1+e_{CIA}}\frac{1}{1+\frac{3}{8}\frac{p}{E}\left(\frac{D_{CIA}}{t_{CIA}}\right)^3},$$

$$\varphi_1 = 1 + \frac{3}{2}\frac{D_{AA}}{t_{AA}}\frac{1-e_{AA}}{1+e_{AA}}\frac{1}{1+\frac{3}{8}\frac{p}{E}\left(\frac{D_{AA}}{t_{AA}}\right)^3}.$$

The dependences of l_{K1} and l_{K2} on the geometry were estimated in the form $l_{K1} = C_1\sqrt{D_{CIA}t_{CIA}}$ and $l_{K2} = C_2\sqrt{D_{AA}t_{AA}}$, where C_1 and C_2 are constants, which were found by comparison with the FE results.

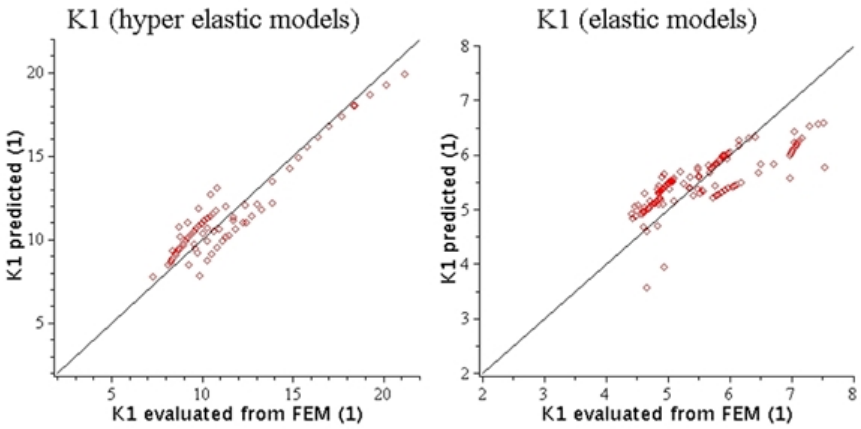

FIGURE 6. A comparison of the K1 values evaluated from FEM and the K1 values calculated by the regression model. The graph on the left represents the set of linearly elastic models, while the graph on the right graph represents the set of hyper elastic models.

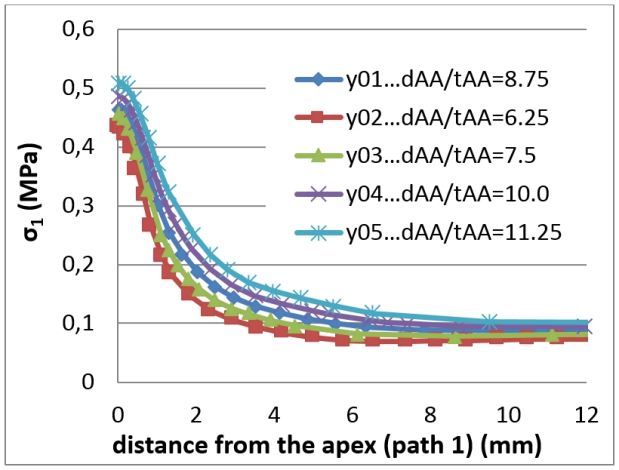

FIGURE 5. Mises stress tracked on path 1. Only the beginnings of the path are displayed. The curves correspond to linearly elastic FE models (y_{01}, y_{02},... y_{05}), where only one parameter (D_{AA}) has been varied. The rest of the geometrical parameters remain constant. The graph shows exact values of the Mises stress under the same loading (pressure 120 mmHg).

3. Results and discussion

Examples of the Mises stress along path 1 are displayed in Figure 5. The graph contains results from linearly elastic variants of five models (y_{01} to y_{05}), in which only D_{AA} varies. The rest of the parameters remain constant.

Tables 2 and 3 summarise the outcomes of a regression analysis.

The prediction ability of regression models of K_1 (for both linearly elastic and hyper elastic materials) are demonstrated by the graphs in Figure 6.

Some results can be interpreted on the basis of an examination of the regression coefficients: when the bifurcation angle decreases by 10°, K_1 increases on an average by 10 %. However, increasing the non-planarity angle also by 10°causes an increase of K_1 on an average by 5 %. Changes of the relative wall thickness have only a slight impact on K_1. It is clear that some factors that have been neglected would affect the stress distribution. For example, a published FE model of AB [35] showed a 15 % increase in SCF when an orthotropic model was used. A 7 % increase in SCF was reported when an orthotropic model was used [16]. According to an FE model of carotid bifurcation [19], the increase in stress within the apex, using an anisotropic model, was about 18 %. However, the prestrain of the arterial wall should reduce the SCF in the apex [20]. Both anisotropy and prestrain have been neglected in our study. A 50 % Increase in the Young modulus of elasticity should increase the SCF in the apex by 7 %, according to [35]. A positive correlation between the Young modulus and K1 has also been evidenced in our study.

3.1. Sizes of the affected regions

Only relatively small regions of the arterial wall are affected by stress concentrators (K_1 and K_2). Lengths l_{K1} and l_{K2} were evaluated to be proportional to constant 1.66 and constant 2.81, respectively:

$$l_{K1} = 1.66\sqrt{D_{CIA}t_{CIA}},$$
$$l_{K2} = 2.81\sqrt{D_{AA}t_{AA}}.$$

3.2. Qualification of the stress in stress concentrations

Six components of the stress both in the apex and in the rear side of AB are shown in Figure 7. We can say that the dominant stress component which the loads the arterial wall within the apex is a normal stress in antero-posterior direction. This stress component is almost equal to the evaluated Mises stress. The dominant stress components in the second stress concentrator are the tangential stress ($= 1.12\sigma_{max2}$) and the axial stress ($= 0.68\sigma_{max2}$). This stress state does not differ dramatically from the state in AA or in CIA far away from AB.

	a_0	a_1	a_2	a_3	a_4	f_0
K_1	−0.95	−0.051	8.18	2.34	1.33	−0.00079
K_2	2.27	−0.022	1.45	2.	—	−0.000057

Table 2. Regression coefficient evaluated from results of (Hooke) linearly elastic FE models.

	a_0	a_1	a_2	a_3	a_4	f_0
K_1	19.7	−0.031	5.17	3.28	−138	−0.00025
K_2	4.7	−0.02	0.082	6.13	—	−0.000023

Table 3. Regression coefficient evaluated from the results of (Odgen) hyper elastic FE models.

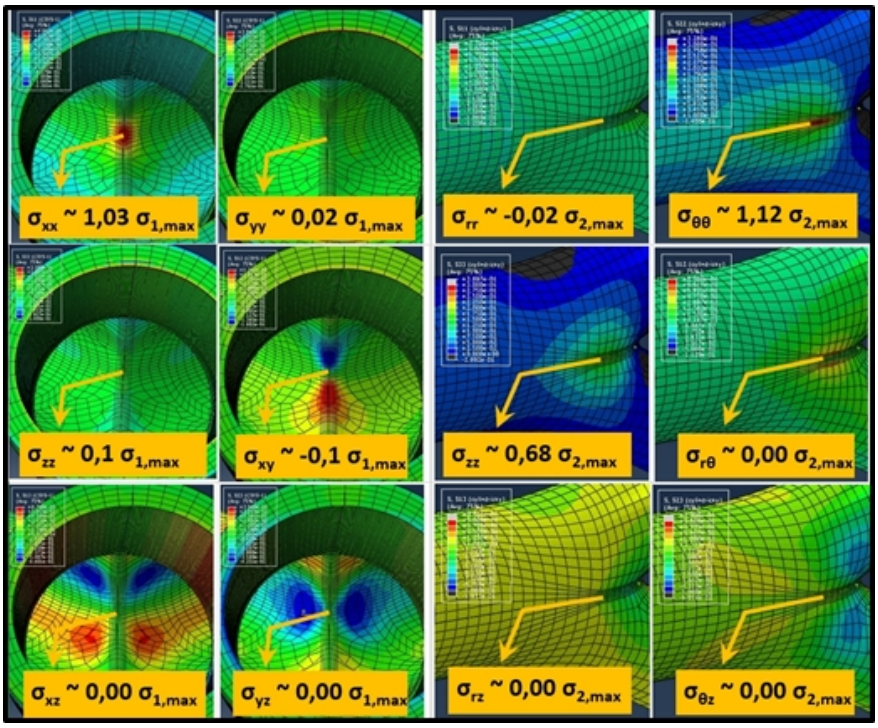

Figure 7. Stress components in the apex (the six pictures on the left) and in the outer rear side (the six pictures on the right). The z axis corresponds to the axis of the aorta; the x axis corresponds to antero-posterior direction; the y axis corresponds to lateral direction; r is the radial coordinate of AA, and Θ means circumferential coordinate. The stress components are expressed as ratios to the Mises stresses ($\sigma_{1,max}$ or $\sigma_{2,max}$).

4. Conclusion

Simple regression models predicting SCF and the size of the affected region in two regions of interest have been proposed. They take into account the geometry, the internal pressure and the material parameters. Simple regression models may be used by physicians for a quick estimate of whether or not the aortic bifurcation of a specific patient poses a high risk due to the high level of mechanical stress. According to the data, the risk is mainly due to a small bifurcation angle and/or a high non-planarity angle. A sharp apex radius also should raise K_1, but this was observed only in a hyper elastic set of models. Both K_1 and K_2 decrease with increasing relative pressure, both in the case of linearly elastic models and in the case of hyper elastic models (but the maximum stress increases with pressure, of course). A positive correlation between the Young modulus and K1 has also been evidenced in our study.

References

[1] J. C. Wang and M. Bennett, "Aging and Atherosclerosis: Mechanisms, Functional Consequences, and Potential Therapeutics for Cellular Senescence," *Circulation Research,* vol. 111, no. 2, pp. 245-259, 2012. doi:10.1161/CIRCRESAHA.111.261388

[2] D. P. Faxon, M. A. Creager, S. C. Smith, R. C. Pasternak, J. W. Olin, M. A. Bettmann, M. H. Criqui, R. V. Milani, J. Loscalzo, J. A. Kaufman, D. W. Jones and W. H. Pearce, "Atherosclerotic Vascular Disease Conference: Executive Summary: Atherosclerotic Vascular Disease Conference Proceeding for Healthcare Professionals From a Special Writing Group of the American Heart Association," *Circulation,* vol. 109, no. 21, pp. 2595-2604, 2004. doi:10.1161/01.CIR.0000128517.52533.DB

[3] R. Beare, G. Das, M. Ren, W. Chong and T. Phan, "Does the principle of minimum work apply at the carotid bifurcation: a retrospective cohort study," vol. 11, no. 1, pp. 1-6, 2011. DOI:10.1186/1471-2342-11-17

[4] C. Taylor, T. Hughes and C. Zarins, "Finite Element Modeling of Three-Dimensional Pulsatile Flow in the Abdominal Aorta: Relevance to Atherosclerosis," *Annals of Biomedical Engineering,* vol. 26, pp. 975-987, 1998. DOI:10.1114/1.140

[5] E. Cecchi, C. Giglioli, S. Valente, C. Lazzeri, G. F. Gensini, R. Abbate and L. Mannini, "Role of hemodynamic shear stress in cardiovascular disease," *Atherosclerosis,* vol. 214, no. 2, pp. 249-256, 2011. DOI:10.1016/j.atherosclerosis.2010.09.008

[6] A. Smedby, "Geometrical Risk Factors for Atherosclerosis in the Femoral Artery: A Longitudinal Angiographic Study," *Annals of Biomedical Engineering,* vol. 26, no. 3, pp. 391-397, 1998. DOI:10.1114/1.121

[7] Y. S. Chatzizisis, A. U. Coskun, M. Jonas, E. R. Edelman, C. L. Feldman and P. H. Stone, "Role of Endothelial Shear Stress in the Natural History of Coronary Atherosclerosis and Vascular Remodeling: Molecular, Cellular, and Vascular Behavior," *Journal of the American College of Cardiology,* vol. 49, no. 25, pp. 2379-2393, 2007. DOI:10.1016/j.jacc.2007.02.059

[8] F. Gijsen, A. van der Giessen, A. van der Steen and J. Wentzel, "Shear stress and advanced atherosclerosis in human coronary arteries," *JOURNAL OF BIOMECHANICS,* vol. 46, no. 2, SI, pp. 240-247, JAN 18 2013. DOI:10.1016/j.jbiomech.2012.11.006

[9] S. Zhao, B. Ariff, Q. Long, A. Hughes, S. Thom, A. Stanton and X. Xu, "Inter-individual variations in wall shear stress and mechanical stress distributions at the carotid artery bifurcation of healthy humans," *Journal of Biomechanics,* vol. 35, no. 10, pp. 1367-1377, 2002. DOI:10.1016/S0021-9290(02)00185-9

[10] S. van Wyk, L. P. Wittberg and L. Fuchs, "Wall shear stress variations and unsteadiness of pulsatile blood-like flows in 90-degree bifurcations," *Computers in Biology and Medicine,* vol. 43, no. 8, pp. 1025-1036, 2013. DOI:10.1016/j.compbiomed.2013.05.008

[11] M. I. Papafaklis, C. V. Bourantas, P. E. Theodorakis, C. S. Katsouras, D. I. Fotiadis and L. K. Michalis, "Association of endothelial shear stress with plaque thickness in a real three-dimensional left main coronary artery bifurcation model," *International Journal of Cardiology,* vol. 115, no. 2, pp. 276-278, 2007. DOI:10.1016/j.ijcard.2006.04.030

[12] X. Kang, "Assessment of the pulsatile wall shear stress in the stenosed and recanalized carotid bifurcations by the lattice Boltzmann method," *Computers & Fluids,* vol. 97, no. 0, pp. 156-163, 2014. DOI:10.1016/j.compfluid.2014.04.011

[13] P. Evegren, L. Fuchs and J. Revstedt, "Wall shear stress variations in a 90-degree bifurcation in 3D pulsating flows," *Medical Engineering & Physics,* vol. 32, no. 2, pp. 189-202, 2010. DOI:10.1016/j.medengphy.2009.11.008

[14] A. Malek, S. Alper and S. Izumo, "Hemodynamic shear stress and its role in atherosclerosis," *Jama-Journal of the American Medical Association,* vol. 282, no. 21, pp. 2035-2042, DEC 1 1999. DOI:10.1001/jama.282.21.2035

[15] S. Wolf and N. Werthessen, "Hemodynamic Contribution to Atherosclerosis," in *Dynamics of Arterial Flow*, vol. 115, S. Wolf and N. Werthessen, Eds., Springer US, 1979, pp. 353-466. DOI:10.1007/978-1-4684-7508-1_7

[16] M. Thubrikar, Vascular Mechanics and Pathology, Springer, 2007. DOI:10.1007/978-0-387-68234-1

[17] R. S. Salzar, M. J. Thubrikar and R. T. Eppink, "Pressure-induced mechanical stress in the carotid artery bifurcation: A possible correlation to atherosclerosis," *Journal of Biomechanics,* vol. 28, no. 11, pp. 1333-1340, 1995. DOI:10.1016/0021-9290(95)00005-3

[18] A. Creane, E. Maher, S. Sultan, N. Hynes, D. J. Kelly and C. Lally, "Finite element modelling of diseased carotid bifurcations generated from in vivo computerised tomographic angiography," *Computers in Biology and Medicine,* vol. 40, no. 4, pp. 419-429, 2010. DOI:10.1016/j.compbiomed.2010.02.006

[19] I. Hariton, G. deBotton, T. Gasser and G. Holzapfel, "How to incorporate collagen fibers orientations in an arterial bifurcation," in *Proceedings of the Third IASTED International Conference on BIOMECHANICS*, 2005.

[20] A. Delfino, N. Stergiopulos, J. M. Jr and J.-J. Meister, "Residual strain effects on the stress field in a thick wall finite element model of the human carotid bifurcation," *Journal of Biomechanics,* vol. 30, no. 8, pp. 777-786, 1997. DOI:10.1016/S0021-9290(97)00025-0

[21] B. Nanayakkara, C. Gunarathne, A. Sanjeewa, K. Gajaweera, A. Dahanayake, U. Sandaruwan and U. de Silva, "Geometric anatomy of the aortic-common iliac bifurcation," *Galle Medical Journal,* vol. 12, no. 1, 2009. DOI:10.4038/gmj.v12i1.1078

[22] P. M. Shah, "Geometric anatomy of the aortic-common iliac bifurcation," *Journal of Anatomy,* vol. 126, no. 3, pp. 451-458, 1978.

[23] C. Bargeron, G. Hutchins, G. Moore, O. Deters, F. Mark and M. Friedman, "Distribution of the geometric parameters of human aortic bifurcations," *Arteriosclerosis, Thrombosis, and Vascular Biology,* vol. 6, no. 1, pp. 109-113, 1986. DOI:10.1161/01.ATV.6.1.109

[24] M. H. Friedman and Z. Ding, "Variability of the planarity of the human aortic bifurcation," *Medical Engineering & Physics,* vol. 20, no. 6, pp. 469-472, 1998. DOI:10.1016/S1350-4533(98)00039-3

[25] P. OFlynn, G. O'Sullivan and A. Pandit, "Geometric Variability of the Abdominal Aorta and Its Major Peripheral Branches," *Annals of Biomedical Engineering,* vol. 38, no. 3, pp. 824-840, 2010. DOI:10.1007/s10439-010-9925-5

[26] J. J. Yeung, H. J. Kim, T. A. Abbruzzese, I. E. Vignon-Clementel, M. T. Draney-Blomme, K. K. Yeung, I. Perkash, R. J. Herfkens, C. A. Taylor and R. L. Dalman, "Aortoiliac hemodynamic and morphologic adaptation to chronic spinal cord injury," *Journal of Vascular Surgery,* vol. 44, no. 6, pp. 1254–1265.e1, 2006. DOI:10.1016/j.jvs.2006.08.026

[27] N. MacLean and M. Roach, "Thickness, taper, and ellipticity in the aortoiliac bifurcation of patients aged 1 day to 76 years," *Heart and Vessels,* vol. 13, no. 2, pp. 95-101, 1998. DOI:10.1007/BF01744592

[28] A. Li, I. Kamel, F. Rando, M. Anderson, B. Kumbasar, J. Lima and D. Bluemke, "Using MRI to assess aortic wall thickness in the multiethnic study of atherosclerosis: Distribution by race, sex, and age," *AMERICAN JOURNAL OF ROENTGENOLOGY,* vol. 182, no. 3, pp. 593-597, 2004. DOI:10.2214/ajr.182.3.1820593

[29] E. B. Rosero, R. M. Peshock, A. Khera, P. Clagett, H. Lo and C. H. Timaran, "Sex, race, and age distributions of mean aortic wall thickness in a multiethnic population-based sample," *Journal of Vascular Surgery,* vol. 53, no. 4, pp. 950-957, 2011. DOI:10.1016/j.jvs.2010.10.073

[30] C. D. Murray, "The Physiological Principle of Minimum Work: I. The Vascular System and the Cost of Blood Volume," *Proceedings of the National Academy of Sciences of the United States of America,* vol. 12, no. 3, pp. 207-214, 1926. DOI:10.1073/pnas.12.3.207

[31] R. W. Ogden, "Large Deformation Isotropic Elasticity - On the Correlation of Theory and Experiment for Incompressible Rubberlike Solids," *Proceedings of the Royal Society of London A: Mathematical, Physical and Engineering Sciences,* vol. 326, no. 1567, pp. 565-584, 1972. DOI:10.1073/pnas.12.3.207

[32] J. Kronek, L. Horny, T. Adamek, H. Chlup and R. Zitny, "Site-Specific Mechanical Properties of Aortic Bifurcation," 2014. DOI:10.1007/978-3-319-00846-2_232

[33] V. Krupka and P. Schneider, Stavba chemických zařízení I Skořepiny tlakových nádob a nádrží, Vysoké učení technické v Brně, 1986.

[34] A. Austin and J. Swannell, "Stresses in a pipe bend of oval cross-section and varying wall thickness loaded by internal pressure," *International Journal of Pressure Vessels and Piping,* vol. 7, no. 3, pp. 167-182, 1979. DOI:10.1016/0308-0161(79)90016-4

[35] L. Manuel, "A Study of the Stress Concentration at the Branch Points of Arteries in Vivo by the Finite Element Method," 1986.